Chapter 69
Experimental Study on Aeroacoustic of Counter-Rotating Propeller in Ground Acoustic Environment

Wei Kai, Cao Qi, Yan Qun, Xu Jian, and Xue Dongwen

Abstract According to the performance evaluation and optimization research requirement of counter-rotating propellers aeroacoustics, based on ground acoustic environment, a set of counter-rotating propeller aeroacoustics test platform was built. The aeroacoustic test of counter-rotating propeller was carried out in a semi-anechoic chamber. The aerodynamic performance and far-field noise characteristics of the counter-rotating propeller were obtained, and the distribution of far-field noise were analyzed. The results show that the tension, torque and power increase with the increase of rotating speed. The amplitude distribution of sound pressure level of far-field noise will move with the change of speed. The discrete noise at each passing frequency is also different. The test platform and the test scheme could provide help for the aeroacoustic evaluation and optimization design of counter-rotating propeller under ground takeoff condition.

Keywords Counter-rotating propeller · Aerodynamics · Far-field noise · Test measurement · Directivity

69.1 Introduction

Compared with turbofan engines of the same thrust level, propeller engines have the advantages of high fuel efficiency and good maneuverability. However, there are disadvantages such as large propeller diameter, complicated mechanism design and low flight speed. Counter-rotating propeller, also known as counter-rotating open rotor, has two rows of propellers with opposite rotation. Two rows of propellers increase the number of blades, and the diameter of blades can be appropriately reduced, so as to increase the cruise Mach number and solve some design difficulties of single row propellers. Some data show that the efficiency of contra-rotating

W. Kai (✉) · C. Qi · Y. Qun · X. Jian · X. Dongwen
Aviation Technology Key Laboratory of Aeroacoustics and Vibration, Aircraft Strength Research Institute of China, Aviation Industry Corporation of China Limited, Xi'an, China
e-mail: weikai.258@163.com

S. Li (ed.), *Computational and Experimental Simulations in Engineering*, Mechanisms and Machine Science 145, https://doi.org/10.1007/978-3-031-42987-3_69

propeller can be improved by 6–16% compared with conventional propeller [1]. However, compared with single-row propellers, the interference noise of contra-rotating propellers and the noise of single propellers lead to huge noise. There is no package in the nacelle, and the noise radiates directly into the cabin and surrounding environment. This seriously limits the application and further development of contra-rotating propellers in the civil market [2–4]. With the rise of oil price and stricter restrictions on carbon emissions and noise, it is urgent to solve the noise problem of contra-rotating propellers.

At present, the main methods to study the noise of contra-rotating propeller are numerical simulation and experimental measurement. In terms of numerical simulation, Envia [5] simulates the unsteady flow field of a contra-rotating rotor by combining computational fluid dynamics (CFD) with computational aeroacoustics (CAA). He used Ffowcs Williams-Hawkings (FW-H) to calculate the far-field noise. The numerical simulation results are in good agreement with the experimental results. The comparison results show that the noise amplitude mainly occurs at the passage frequency and its harmonics of the two rows of blades. GE [4] optimized and designed a low-noise contra-rotating open rotor model based on the blades of GE36 open rotor engine. GE uses the self-developed CFD-CAA software to simulate the aerodynamic and noise performance of the open rotor under cruise conditions, and the results are good. In terms of test measurement, Parrya [7] described the wind tunnel tests of three typical contra-rotating propellers, and analyzed the distribution characteristics of discrete noise and broadband noise in detail. NASA, GE, TsAGI and other laboratories have established the aerodynamic noise test bench of contra-rotating propeller in the wind tunnel. They have successively carried out aerodynamic noise tests in low-speed wind tunnels, high-speed wind tunnels and acoustic wind tunnels, and obtained a large number of test data. These test data guide the subsequent aerodynamic noise optimization design of contra-rotating propeller [8–10].

In the 1980s, GE developed the GE36-UDF open-rotor engine and carried out test flight on the MD-80 aircraft. The test results show that the noise level of this type of engine meets the noise requirements of the third stage of ICAO. Compared with the original engine, the noise and vibration levels are reduced [11–13]. At the same time, Loma designed SR-7 pair of rotor fans and also carried out flight tests [14, 15]. In 2022, the China Aerodynamic Research and Development Center set up an aerodynamic noise test platform for contra-rotating propellers. In the acoustic wind tunnel, the aerodynamic performance and aerodynamic noise tests of contra-rotating propellers were carried out. At the same time, the influence of the rear rotor diameter on the aerodynamic and noise of the contra-rotating propeller is studied by numerical simulation.

The BeiHang University has built a small aerodynamic noise test rig for contra-rotating propellers in the anechoic chamber. The platform uses two motors to drive two rows of propellers, and the flow mechanism between the two rows of propellers is preliminarily studied [16, 17]. Ning and Hu [18] tested the noise of a UAV propeller in the anechoic chamber and evaluated the impact of the blade serrated trailing edge on the noise. Mariono [19] measured the acoustic characteristics of the propeller under different propulsion ratios in the anechoic chamber, and analyzed the noise

characteristics of the propeller under zero propulsion ratio, but the error was large. The aerodynamic noise test in wind tunnel or flight platform is costly and difficult to control the time schedule, which is the obstacle faced by the current research on the aerodynamic noise of contra-rotating propeller. The above aerodynamic noise test scheme in the anechoic chamber can be used for reference, but the test design needs to be improved to reduce the error.

In this paper, a set of aerodynamic noise test platform for contra-rotating propeller is designed. For a set of contra-rotating propellers, the aerodynamic noise test research was carried out at different speed conditions. The aerodynamic performance and far-field noise characteristics of the counter-rotating propeller are evaluated.

69.2 Experimental Principle

The purpose of this test is to evaluate the aerodynamic performance and far-field noise characteristics of counter-rotating propellers. By measuring the pulling force, torque and other parameters of the contra-rotating propeller. The pull coefficient and torque coefficient of the propeller are calculated by formulas (69.1)–(69.4). The aerodynamic performance of counter-rotating propeller can be evaluated according to the above parameters.

$$C_T = \frac{T}{\rho n_s^2 D^4} \tag{69.1}$$

$$C_M = \frac{M}{\rho n_s^2 D^5} \tag{69.2}$$

$$P = 9549 \frac{M}{\mathrm{n}} \tag{69.3}$$

$$C_P = \frac{P}{\rho n_s^3 D^5} \tag{69.4}$$

where T is trust, M is torque, C_T is trust coefficient, P is power, and C_P is power coefficient. ρ is the air density, n_s is the propeller rotation speed (r/s), D is the propeller diameter, n is the speed (r/min), and P is the power.

The noise source of contra-rotating propeller is the same as that of single-row propeller, which has obvious directionality. Take the rotation center of the rear row blades of the counter rotating propeller as the origin. The sound intensity of the far-field noise receiving point can be recorded as I, and the average sound intensity of other points at the same distance can be recorded as $\overline{I}$. Then the directivity factor Q and directivity index DI are defined as:

$$Q = \frac{I}{\overline{I}} \tag{69.5}$$

$$DI = 10 \lg Q = L_{p\theta} - \overline{L}_p \tag{69.6}$$

where $L_{p\theta}$ is the sound pressure level at angle θ on the spherical surface with radius r; $\overline{L}_p$ is the average sound pressure level measured on the spherical surface with radius r. The directivity index can usually be measured directly. In three-dimensional spherical coordinates, the directivity index $DI(\theta, \varphi)$ in a specific direction has the following relationship with the sound pressure level $L_p(r, \theta, \varphi)$ measured at the distance r.

$$Q(\theta, \varphi) = \lg^{-1} \frac{DI(\theta, \varphi)}{10} \tag{69.7}$$

The directivity index of sound source in the ground acoustic environment can be considered as a free field on the reflecting surface, and the directivity index is:

$$DI = L_{pi} - \overline{L}_p + 3 \tag{69.8}$$

where W is the sound pressure level at the distance R from the sound source; E is the average sound pressure level on the test hemisphere. Through formula (69.8), the fluctuation of sound pressure level at each measuring point in the far field relative to the average level is given. In this paper, the noise characteristics of the contra-rotating propeller will be evaluated by the spectrum and directivity of the far-field noise.

69.3 Experimental Device and Scheme

69.3.1 Experimental Platform

With the semi-anechoic chamber as the ground acoustic environment, a set of anti-rotating propeller aerodynamic noise test platform is built, and the schematic diagram is shown in Fig. 69.1. The test platform includes base, slide rail, servo motor, tension sensor, torque sensor, cooling system and control system. The servo motor drives the propeller to rotate through the coupling and gearbox. The tension sensor is installed on the slide rail to measure the tension transmitted by the contra-rotating propeller when it rotates. The torque sensor is connected with the coupling to measure the torque transmitted by the contra-rotating propeller. The base is designed as a streamlined shape, which can reduce the airflow disturbance caused by the test bed. The tester shall measure and control outside the semi-anechoic chamber to ensure safety.

The maximum rotational speed of the contra-rotating propeller test platform is 3500 rpm, the tension measurement range is 0–400 N, and the torque measurement range is 0–400 Nm.

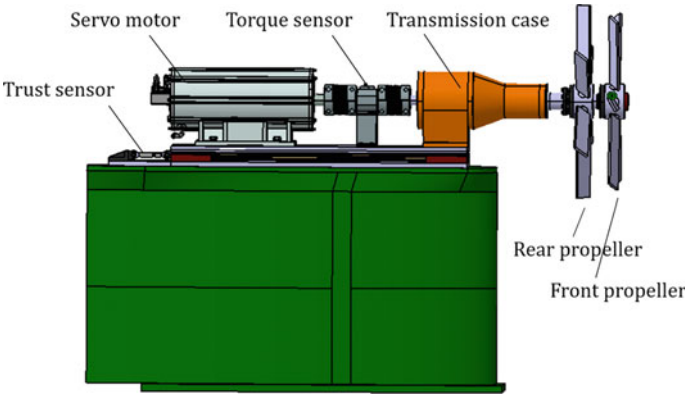

Fig. 69.1 Schematic diagram of test platform

69.3.2 Experimental Conditions

This test was carried out in the semi-anechoic chamber of the China Aircraft Strength Research Institute. The size of the semi-anechoic chamber is 10 * 10 * 8 m. The test site is shown in Fig. 69.2. The test items include aerodynamic performance test and far-field noise test. The diameter of the contra-rotating propeller is 0.66 m, and there are 6 blades in the front and rear rows. The blades are made of composite materials. NACA0012 airfoil is selected as the blade, and the blade angle at 70% blade height is 20°. Based on the similarity of blade tip Mach number and the ground takeoff condition, the test condition is designed. The rotational speed is set at 1500, 2000, 2500, 2600, 2800 and 3000 rpm, and the relationship between the rotational speed and the aerodynamic performance of the contra-rotating propeller and the far-field noise is studied.

69.3.3 Test Method

The purpose of aerodynamic performance test is to obtain the pull and torque of the contra-rotating propeller. After the test reaches the preset working condition, the tension and torque can be directly read from the control system. A microphone array is arranged in the semi-anechoic chamber to measure the sound pressure at each noise observation point in the far field. The microphone array arrangement is shown in Fig. 69.3.

The microphone array is composed of 12 BK4954 free-field microphones with a distance of 10°. The microphone is uniformly distributed on the circular arc with the rotation center of the rear row propeller as the center and the radius of 3.5 m. The height of the microphone is consistent with the rotation center of the propeller. During the test, the microphone is equipped with a windproof ball in order to reduce the error

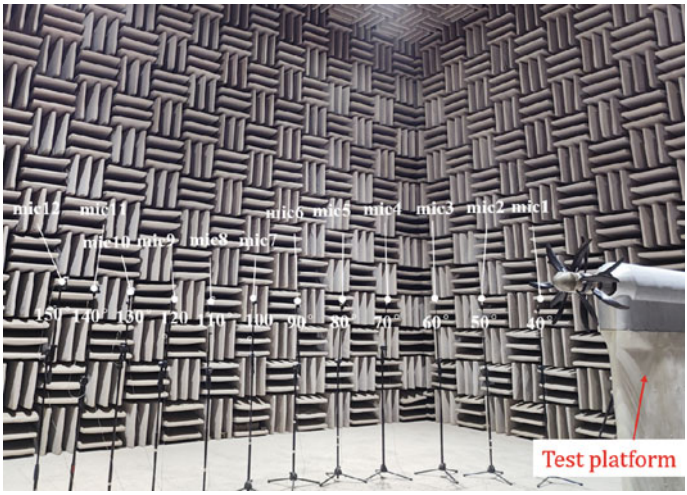

Fig. 69.2 Test site photo

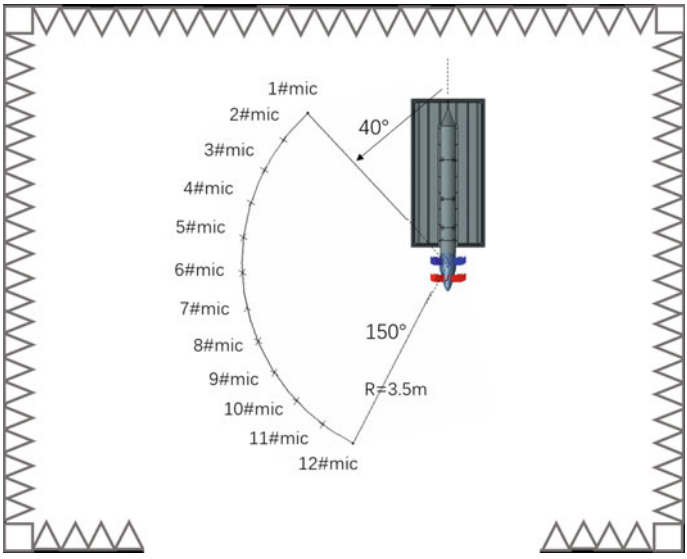

Fig. 69.3 Schematic diagram of microphone array

caused by the rotating turbulence of the propeller. During the test, 12 microphones simultaneously collected 20 s of sound pressure data. The adopted frequency is set at 16384 Hz, and the microphone must be calibrated.

69.4 Experimental Results and Analysis

The test results include aerodynamic performance results and far-field noise results. The aerodynamic performance results are directly measured tension, torque, power and indirectly calculated tension coefficient, torque coefficient and power coefficient. The far field noise is mainly noise frequency spectrum and directivity.

69.4.1 Aerodynamic Results and Analysis

Figure 69.4 shows the test results of the pull force of the counter-rotating propeller at different speeds. It can be seen that the pulling force increases with the increase of rotating speed, and the increase is large. No stall occurs within the measured speed range. Figure 69.5 shows the change of the tension coefficient with the speed. The tension coefficient increases with the increase of the speed, and the increase slows down after 2800 rpm. The tensile force and the coefficient of tensile force increase with the increase of the rotating speed, which indicates that the blade angle and the rotating speed match well in the whole test rotating speed range.

Figure 69.6 shows the torque test results, and Fig. 69.7 shows the torque coefficient results. As can be seen from Fig. 69.6, with the increase of speed, the torque also increases, but the growth rate is small. It can be seen from Fig. 69.7 that the torque coefficient decreases with the increase of speed. From 1500 to 2000 rpm, the torque coefficient decreases greatly; The decrease from 2000 to 3000 rpm slowed down. This shows that in the speed range of 1500–2000 rpm, the matching degree between blade angle and speed is high.

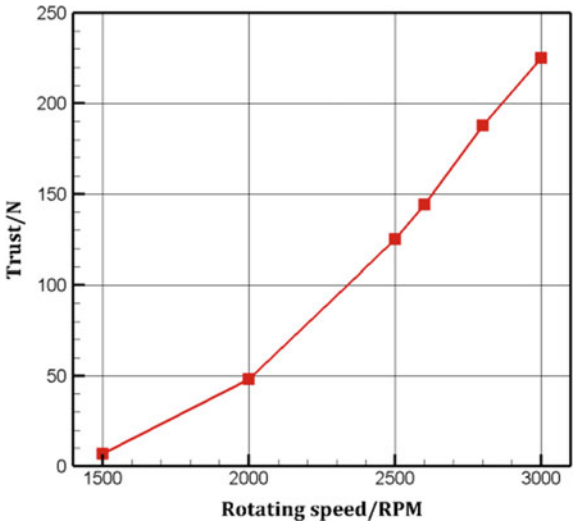

Fig. 69.4 Thrust data of test

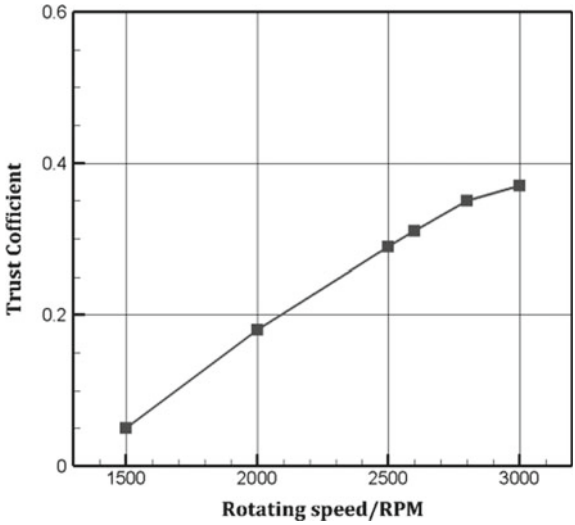

Fig. 69.5 Thrust coefficient data of test

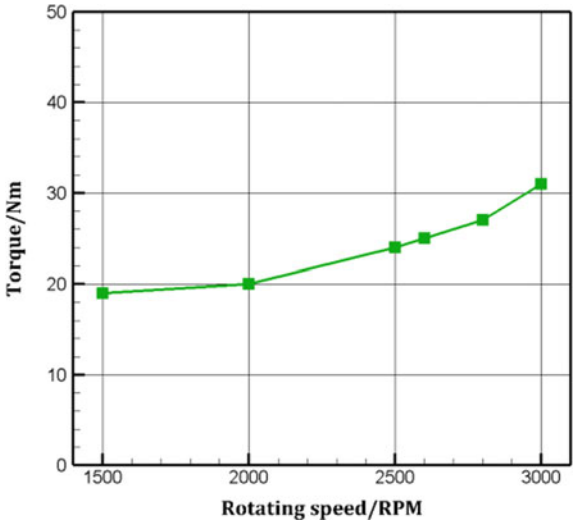

Fig. 69.6 Torque data of test

Figures 69.8 and 69.9 show the relationship between the power, power coefficient and rotational speed of the contra-rotating propeller. It can be seen from Fig. 69.8 that the power increases with the increase of speed, and the increase is obvious. It can be seen from Fig. 69.9 that the power coefficient decreases with the increase of the speed, and the speed of decline is fast in the range of 1500–2000 rpm; In the range of 2000–3000 rpm, the power factor slows down with the speed of speed reduction. These results show that in the speed range of 1500–2000 rpm, the matching degree of blade angle and speed is high, which is consistent with the conclusion in Fig. 69.7.

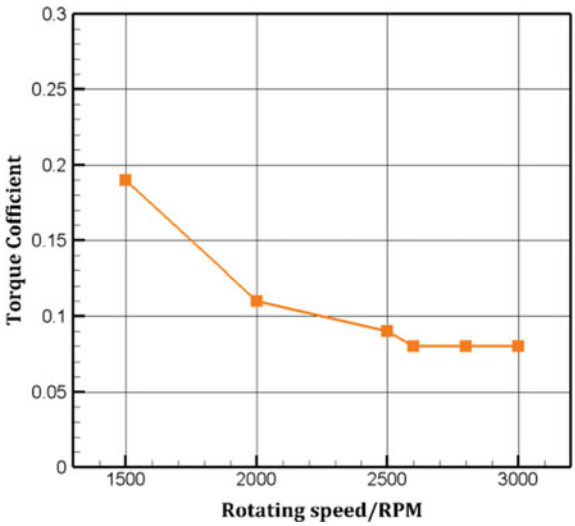

Fig. 69.7 Torque coefficient data of test

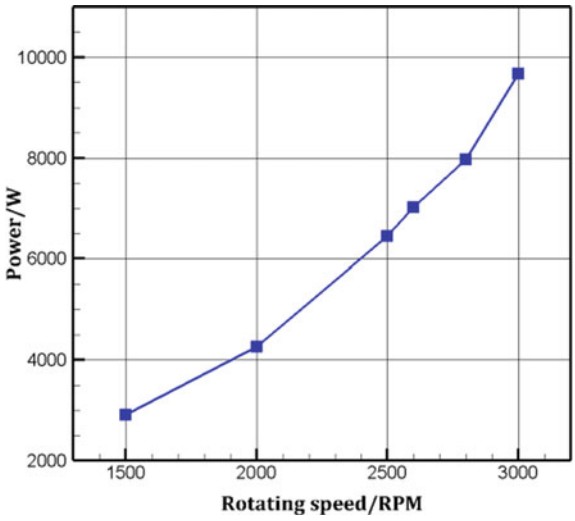

Fig. 69.8 Power data of test

The aerodynamic performance of the contra-rotating propeller is obtained through experiments, which provides a basis for the optimal design of the blade. The aerodynamic noise optimization of contra-rotating propellers is similar to that of single-row propellers. Even when the efficiency of propellers is guaranteed, the noise is minimal. According to the required power and tension requirements, the airfoil of the blade is initially selected and the number of blades is determined.

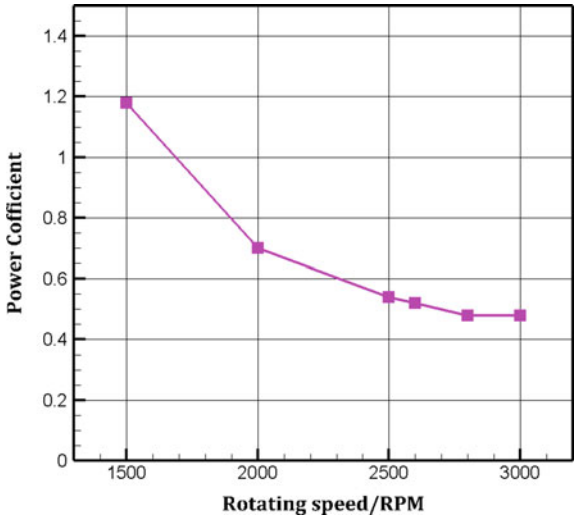

Fig. 69.9 Power coefficient data of test

69.4.2 Noise Results and Analysis

The far-field noise spectrum of the counter-rotating propeller at 3000 rpm is shown in Fig. 69.10. It can be seen from Fig. 69.10 that the far field noise amplitude of the contra-rotating propeller in this test is within 3000 Hz, and the higher frequency band is mainly broadband noise. The results accord with the general law of aerodynamic noise of contra-rotating propeller.

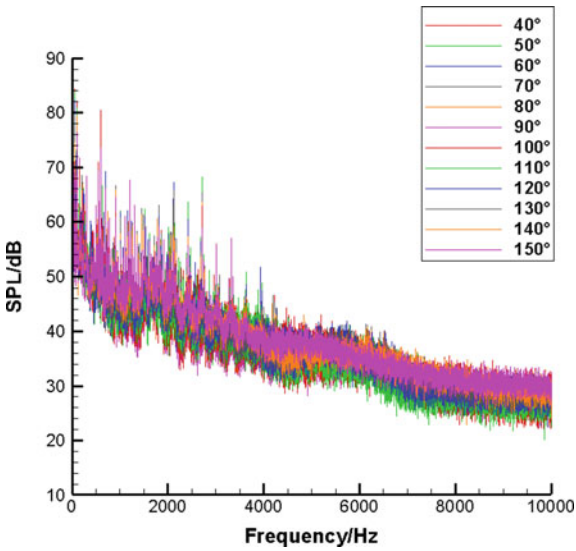

Fig. 69.10 Spectra of far-field noise of different azimuthal angles at 3000 rpm

Figure 69.11 shows the noise spectrum of the counter-rotating propeller at the blade passing frequency (BPF). It can be seen that the noise amplitude at the second pass frequency (2BPF) is greater than that at the first pass frequency (1BPF) and the third pass frequency (3BPF). The amplitude of aerodynamic noise of counter rotating propeller mainly appears at 1BPF, 2BPF and 3BPF, indicating that the noise of counter rotating propeller is mainly discrete noise. The discrete noise mainly comes from the load noise of the single row propeller and the interference noise generated by the interaction between the two rows of propeller. The interference noise of counter-rotating propeller is generated at the interference frequency. The interference frequency is the sum of the passing frequencies of the two rows of propellers and their higher-order harmonics. 2BPF is the first order interference frequency, where the noise amplitude is the largest, which conforms to the general law of aerodynamic noise of contra-rotating propeller. The noise amplitude points of the contra-rotating propeller can be obtained, and the noise reduction method can be put forward in combination with the interference noise generation mechanism.

Figure 69.12 shows the far-field noise directivity results of the counter-rotating propeller at 3000 rpm. It can be seen from the figure that compared with 1BPF and 3BPF, the noise sound pressure level at 2BPF is the highest. Compared with other pointing angles, the sound pressure level at 40° is the highest, followed by 90°, which is also the direction with the greatest impact on the environment and cabin. The noise in the range of 110–150° is low. The noise sound pressure level of 1BPF and 2BPF is small, and the direction of the maximum sound pressure level is around 80°, which is slightly forward compared with 3BPF.

From the previous test results, the noise amplitude of the counter-rotating propeller is mainly at 2BPF, which is interference noise. Then, the noise rule at 2BPF can be

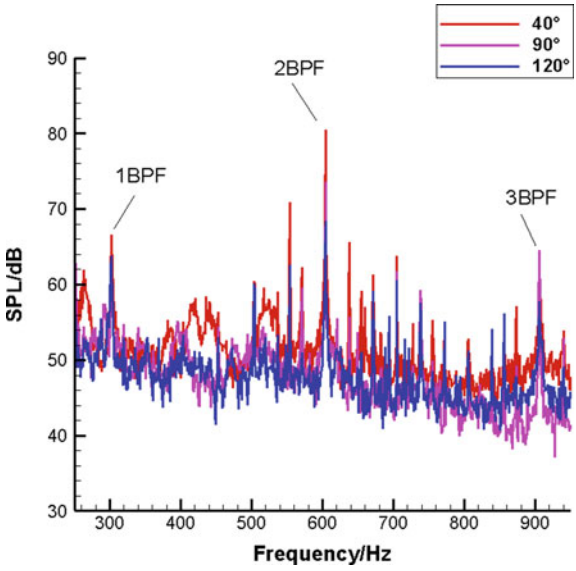

Fig. 69.11 Spectrum at blade passing frequency

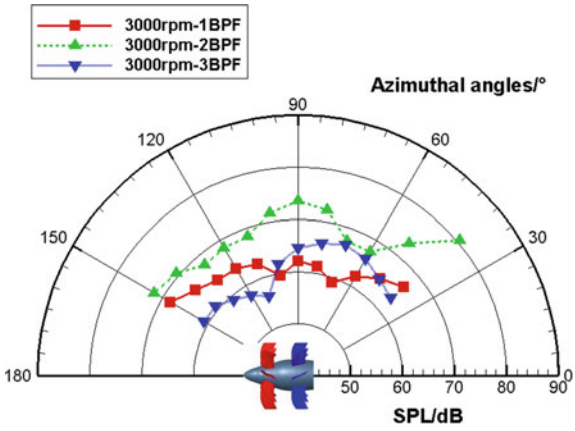

Fig. 69.12 Noise directivity at blade passing frequency—3000 rpm

analyzed through Fig. 69.13. The distribution trend of far-field noise at 2800 and 3000 rpm is similar at each direction, and the amplitude of sound pressure level is the largest at 90° and 40°. The distribution of sound pressure level at 2500 rpm at each direction angle is not consistent with the trend of 2800 and 3000 rpm.

Similar to the generation mechanism of discrete noise of single-row propeller, the discrete noise of counter-rotating propeller is also the result of the propeller periodically cutting the air in the flow field and interacting with it. The noise power is generally the highest in the tip area, so the aerodynamic load can be moved to the inner diameter direction along the peak value of the spanwise distribution to reduce the load noise. The propeller load noise can be reduced by improving the spanwise blade shape or increasing the radial blade width, so as to reduce the discrete noise. On the other hand, the air flow interference between two rows of propellers produces interference noise, which can be reduced in mechanism by adjusting the ratio of the height of two rows of blades or the spacing between two rows of propellers.

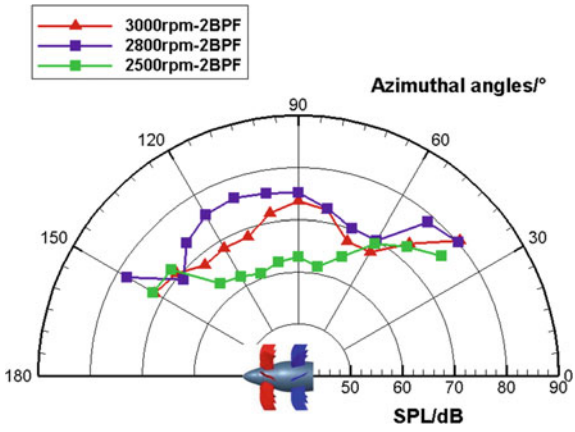

Fig. 69.13 Noise directivity at 2BPF at different speeds

69.5 Conclusion

Within the measured speed range, the pull, torque and power of the counter-rotating propeller increase with the increase of the speed. The torque coefficient and power coefficient decrease with the increase of speed, which indicates that there is still room for optimization of the speed design of the contra-rotating propeller. Interference noise is the main noise of contra-rotating propeller. The aerodynamic noise test platform of contra-rotating propeller can be used to evaluate the aerodynamic noise performance of contra-rotating propeller. The load noise can be reduced by improving the spanwise or radial width of the blade. The interference noise is reduced by adjusting the diameter ratio and pitch of the two rows of propellers.

References

1. Hager, R., Vrabel, D.: Advanced turboprop project. NASA SP-495 (1988)
2. Zhou, L., Shi, J., Wang, Z.: Research progress in open-rotor engine. J. Propuls. Technol. **40**(7), 1921–1932 (2019). (in Chinese)
3. Kingan, M.J., Parry, A.B.: Acoustic theory of the many bladed contra-rotating propeller: the effects of sweep on noise enhancement and reduction. J. Sound Vib. **468**, 89–115 (2020)
4. Parry, A.B., Kingan, M.J.: Acoustic theory of the many bladed contra-rotating propeller: physics of the wake interaction noise critical sources. J. Fluid Mech. **880**, 1–12 (2019)
5. Envia, E.: Contra-rotating open rotor tone noise prediction. In: Proceedings of the AIAA/CEAS Aeroacoustics Conference, AIAA, Atlanta, GA, pp. 1027–1042 (2014)
6. Van Zante, D.E., Collier, F., Orton, A.: Progress in open rotor propulsors: The FAA/GE/NASA open rotor test campaign. Aeronaut. J. **118**(1208), 1181–1213 (2014)
7. Parrya B. Relative importance of open rotor tone and broadband noise sources //Proceedings of 17th AIAA/CEAS Aeroacoustics Conference. Portland, OR: AIAA, 2011:1075–1087.
8. Hoff, G.E.: Experimental Performance and Acoustic Investigation of Modern, Counterrotating lade Concepts. NASA CR 182158, January 1990
9. Elliott, D.M.: Initial Investigation of the Acoustics of a Counter Rotating Open Rotor Model with Historic Baseline Blades in a Low Speed Wind Tunnel. AIAA-2011-2760 (2011)
10. Dale, E., Van, Z.: The NASA Environmentally Responsible Aviation Project/General Electric Open Rotor Test Campaign. AIAA-2013-0415 (2013)
11. GE36: Design and Systems Engineering. Full scale technology demonstration of a modern counter rotating unducted fan engine concept: design report. NASA CR 180867, January 1987
12. GE36: Design and Systems Engineering. Full scale technology demonstration of a modern counter rotating unducted fan engine concept: component test. NASA CR 180868, January 1987
13. GE36: Design and Systems Engineering. Full scale technology demonstration of a modern counter rotating unducted fan engine concept: engine test. NASA CR 180869, January 1987.
14. Little, B.H., Poland, D.T., Bartel, H.W., et al.: Propfan Test Assessment (PTA): Final Project Report. NASA-CR-185138 (1989)
15. Little, B.H., Bartel, H.W., Reddy, N.N., et al.: Propfan Test Assessment (PTA): Flight Test Report. NASA-CR-182278 (1989)
16. Chen, Z., Jiang, Y., Zhao, Y., et al.: The counter-rotating propellers aerodynamic and aerodynamic noise test technology in wind tunnel. J. Aerosp. Power. https://doi.org/10.13224/j.cnki.jasp.20220476
17. Cui, P., Tong, F., Feng, H., et al.: Influence of rear rotor diameter on aerodynamic and acoustic characteristics of counter-rotating propeller. J. Aerosp. Power **37**(8), 1749–1760 (2022)

18. Ning, Z., Hu, H.: An experimental study on the aerodynamics and aeroacoustic characteristics of small propellers of UAV. In: 54th AIAA Aerospace Sciences Meeting. AIAA 2016-1785, San Diego, USA (2016)
19. Marino, L.: Experimental analysis of UAV propeller noise. In: 16th AIAA/CAES Aeroacoustics Conference, Stockholm, Sweden (2010)